Soft Matter

PAPER

Intracellular trafficking of cationic liposome–DNA complexes in living cells†

Stefano Coppola,[a] Laura C. Estrada,[b] Michelle A. Digman,[b] Daniela Pozzi,[a] Francesco Cardarelli,[c] Enrico Gratton[b] and Giulio Caracciolo*[a]

Three-dimensional single-particle tracking (SPT) was used to calculate the mean square displacement (MSD) and the diffusion coefficients of multicomponent cationic liposome–DNA complexes (lipoplexes) in CHO-K1 living cells. In untreated (NT) control cells, we found that the intracellular lipoplex motion was either directed or Brownian with active transportation being definitely more frequent (more than 70%) than Brownian diffusion. The MSD analysis was supported by the calculation of the three-dimensional asphericity, A_3, which was close to unity, denoting the preponderant occurrence of movement along a direction. To elucidate the role of the cytoskeleton structure in the lipoplex trafficking, cells were treated with cytoskeleton (actin microfilaments and microtubules) polymerization inhibitors (latrunculin B and nocodazole, respectively). When cells were treated with inhibitors, the lipoplex movement tended towards a random walk at the expense of directed motion. The disassembly of microtubules had a stronger effect on the reduction of directional movement than that of actin microfilaments. Relevance of the results for enhanced gene delivery is discussed.

Introduction

First proposed over thirty years ago,[1] gene therapy has gained significant attention as a potential method for treating genetic disorders such as severe combined immunodeficiency,[2] cystic fibrosis[3] and Parkinson's disease[4] as well as an alternative method to traditional chemotherapy used in treating cancer.[5] This approach is based on the principle of correcting the basis of diseases at their origin by delivery and subsequent expression of exogenous genetic material.[6] Initial research concentrated on using viral carriers, including both retroviruses and adenoviruses, as these vectors exhibited high efficiency in delivering both DNA and RNA to several cell lines. After the pioneering discovery by Felgner *et al.*[7] that cells can be efficiently transfected by cationic liposome–DNA complexes (lipoplexes), the field of non-viral gene delivery was set aside for a long time, but it has recently seen a renaissance due to the severe concerns connected with the use of viral vectors.[8–10] As a result, cationic lipids, polymers, dendrimers, and peptides gained great attention

because they are non-immunogenic, not oncogenic, easy to produce on a large scale, and capable of delivering large genetic material.[11,12] However, unlike viral analogues that have evolved to overcome cellular barriers and immune defense mechanisms,[13,14] non-viral gene carriers consistently exhibit significantly lower transfection efficiency (TE) compared to viral ones. Lipoplexes are among the most promising nanovectors for gene delivery. A variety of intracellular barriers must be overcome to deliver exogenous DNA into the cell nucleus of the host cell to allow its expression. Lipoplexes must cross the plasma membrane,[15,16] move through the cytoplasm, enter the nucleus, and then release their gene payload for DNA transcription. The intracellular movement of lipoplexes affecting gene delivery may represent one of the major barriers, and remains to be explored. Lukacs *et al.* showed that molecules of naked DNA larger than 2000 bp are unable to diffuse freely in the highly crowded cytoplasm.[17] However, it is known that despite this apparent inability of plasmids to diffuse through the cytoplasm, transfections do result in expression. Trafficking of viral gene vectors has been studied more intensively. Recent studies have pointed to the use by viruses of the cytoskeleton to facilitate transport towards the nucleus.[18,19] Although microtubules appear to be the dominant highways for viruses, they are by no means the exclusive route. In fact, Van Loo *et al.* showed that baculovirus uses the actin cytoskeletal network to move towards the nucleus.[18]

The aim of our work was therefore to provide novel insights into the mechanism of intracellular trafficking of cationic liposome–DNA complexes. This is a fundamental step towards identifying novel strategies for enhanced lipid-mediated gene

[a] *Department of Molecular Medicine, "Sapienza" University of Rome, Viale Regina Elena 324, 00161 Rome, Italy. E-mail: giulio.caracciolo@uniroma1.it*

[b] *Laboratory for Fluorescence Dynamics, Department of Biomedical Engineering, University of California, 3120 Natural Sciences 2, Irvine, California 92697-2715, USA*

[c] *Center for Nanotechnology Innovation, @NEST, Istituto Italiano di Tecnologia, Piazza San Silvestro 12, 56127 Pisa, Italy*

delivery. Three-dimensional (3D) single-particle tracking (SPT) techniques represent a powerful tool for the study of intracellular vesicle transport.[20–23] These fluorescence microscopy techniques were developed to follow the position of individual particles in time. Provided that the spatial and temporal resolution of the method is adequate, SPT trajectories can be analyzed statistically to extract quantitative information regarding the mechanism involved in the motion of a particle. The major advantage of SPT with respect to other fluorescence microscopy techniques developed to measure the motion of particles (for instance, fluorescence recovery after photobleaching (FRAP) and fluorescence correlation spectroscopy (FCS)) is that several transport mechanisms can be detected simultaneously. In the present work, three-dimensional SPT was applied to investigate the intracellular trafficking of multicomponent (MC) lipoplexes in CHO-K1 living cells. This cell line was chosen due to its common use in biological and medical research. Indeed, CHO-K1 cells are among the most widely used mammalian cells for transfection, expression, and large-scale recombinant protein production. Thus, the conclusions of our work are expected to be of broad general interest. MC lipoplexes have been proved to be superior in TE with respect to commonly used binary lipoplexes and completely non-cytotoxic. Due to these peculiar characteristics MC lipoplexes represent promising candidates for gene delivery applications both *in vitro* and *in vivo*.[24–29] To understand the role of cytoskeleton in intracellular trafficking of gene vectors, selective drug treatments are usually performed. While being a very effective method, pharmacological treatment of cells with cytoskeleton-destabilizing drugs can affect cell functions. In order to avoid cell damage potentially caused by drug treatment, nanocarriers and cytoskeleton structure can simultaneously be visualized by multiple labeling. The use of fluorescent probes is among the most powerful techniques for gaining spatial and temporal knowledge of dynamic events within living cells. Unfortunately, multiple labeling fluorescence data are often difficult to analyze because of the cross-talking signal between fluorophores. In addition, fluorescence imaging with multi-color fluorescent markers suffers from having a relatively poor spatial resolution limited to approximately 200 nanometers. It follows that the accurate 3D rendering of confocal images aimed at determining whether vectors are in contact with cytoskeleton structure is not a trivial operation and can possibly lead to misinterpretation. As a consequence, the inhibition of cytoskeleton organization remains the most validated strategy for analyzing the functional role of cytoskeleton. In this study, we took advantage of this approach by using inhibitors of polymerization of actin or microtubule networks. Latrunculin B (LAT) treatment disrupted the actin network, while the microtubule network was disassembled by nocodazole (NCZ). Here we show that both actin filaments and microtubules affect the intracellular trafficking of multicomponent lipoplexes. In untreated (NT) control cells, the intracellular lipoplex motion was mainly directed. Inhibition treatments made the percentage of directional movement decrease, with a simultaneous increase in the occurrence of Brownian motion. The effect of nocodazole on the reduction of directional movement was definitely stronger than that of latrunculin B. This indicates that, even though both types of cytoskeleton could play a role in gene delivery, microtubules are the preferential network for the active transport of cationic liposome–DNA complexes.

Results

We obtained 102 single-particle trajectories that can be divided into three different categories: (i) 57 NT trajectories: lipoplexes tracked in CHO-K1 cells not treated (NT) with inhibitors; (ii) 25 LAT trajectories: lipoplexes tracked in CHO-K1 cells after treatment with latrunculin B; (iii) 20 NCZ trajectories: lipoplexes tracked in CHO-K1 cells treated with nocodazole. Representative NT, LAT and NCZ trajectories are reported in Fig. 1 (the ESI† reports all trajectories). A qualitative analysis of the trajectories reported in Fig. 1 allows us to notice that: (i) NT trajectories are made of almost linear fragments largely displaying unidirectional movement, *i.e.* directed motion; (ii) in LAT trajectories linear fragments, like those found in NT cells, are concomitant with 'ball-of-yarn'-like fragments; and (iii) in NCZ trajectories the apparent percentage of non-linear
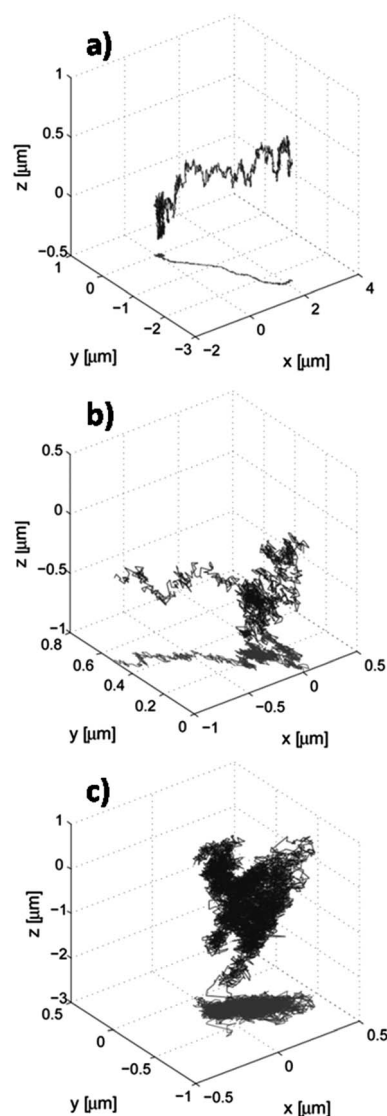
Fig. 1 Representative NT (a), LAT (b) and NCZ (c) trajectories (black). To facilitate the visualization, the *x* and *y* projection of each trajectory is also shown (grey). The position unit on each axis is μm. The time resolution is 32 ms.

fragments seems to increase with respect to the previous two categories. To prove these qualitative observations it is mandatory to introduce a quantitative analysis based on the calculation of the mean square displacement and the gyration tensor.

Mean square displacement

We calculated the one-dimensional mean square displacements following eqn (1)–(3) and setting the maximum value of n to $N/10$ (see Experimental methods). Fig. S20 in the ESI† shows all the 102 MSD curves. The varying range of the maximum time lags shows the wide range of trajectory lengths. This depends on the tracking routine that can lose track of the particle. However, the MSD curves along x and y lie one on top of the other in the same interval $[0, 0.2]$ μm² suggesting that the dynamic parameters such as the diffusion coefficient and the velocity are highly comparable. In contrast, the MSD curves along z lie in a larger interval $[0, 0.55]$ μm² suggesting higher values of the diffusion coefficients and velocities with the respect to the ones obtained from the other spatial directions. This discrepancy might arise from lower measurement accuracy along the z-axis. We estimate an accuracy of 50–100 nm along the vertical axis compared to about 2–20 nm in the x and y plane.[36] Alternatively, these observations could be due to the three dimensional biological structure of the cytoplasm.

The next step of the analysis involves the division by type (Brownian diffusion, confined and directed motion) according to the algorithm proposed. The maximum time lag m is set to $m = 49$ (or still $N/10$ when $N/10 < 49$) with the purpose of keeping the uncertainty small as described in the Experimental methods section. The percentages of each mode of motion are listed for each category in Table 1. These results confirm the initial qualitative analysis by eye. More precisely, with respect to NT cells the percentage of directed motion decreases evidently in LAT-treated cells and even more evidently in NCZ-treated cells. By contrast, the percentage of Brownian motion increases with respect to NT cells in LAT cells and even more in NCZ cells. These two trends are not exactly complementary due to the presence of a small percentage of confined motion (9 MSD curves over a total number of 102 MSD curves). These observations are valid only for the analysis along x and y. In fact, in the z analysis the percentages trend is not so clear. The percentage of Brownian motion is higher (>90%) than in the x and y analysis suggesting the lack of an active transport mechanism along z inside the

cytoplasm. Again, this might reflect the different spatial resolution along the optical axis.

Following the theoretical expressions of eqn (4)–(6), it is possible to perform the (unweighted) fitting of the MSD curves, already divided by type. In Table 2 the average values of the desired physical parameters (D, L and v) are listed. When taking into account the relatively large standard deviations, no specific trend for the mean diffusion coefficient seems to emerge. This observation refers to all the motion types (i.e. D and B) and categories (i.e. NT, LAT and NCZ) in the x and y analysis. The absence of a specific trend could be partly due to the relatively small number of elements to average that might cause a large standard deviation. Alternatively, according to the Stokes–Einstein relation, it might reflect the polydispersity in the size of lipoplexes. Again as a consequence of the different spatial resolution along the optical axis, it is possible to notice the higher average values of the physical parameters in the z direction.

Finally, we consider the short-term diffusion coefficients following the $D(0;4)$ definition, i.e. the slope of a linear fit of the first 5 MSD points. Fig. 2 collects for each category (NT, LAT, NCZ) the short-term diffusion coefficients along x and y. Instead of the number of coefficients for each bin we only show the fraction because it makes the results obtained with this analysis clearer.

Lastly, in the NCZ histograms the peaks keep moving lying in the intervals $D_x = [1, 1.25] \times 10^{-3}$ μm² s⁻¹ and $D_y = [1.25, 1.5] \times 10^{-3}$ μm² s⁻¹. These values are in quite good agreement with those reported in Table 2. In both LAT and NCZ histograms a small peak in the bin $[0, 2.5] \times 10^{-4}$ μm² s⁻¹ still survives denoting the existence of a non-zero fraction of slow particles.

Gyration tensor

Given all the 102 trajectories, it is possible to calculate the gyration tensor and diagonalising it the principal radii of gyration for each category (NT, LAT, NCZ). For the sake of conciseness, only the average values $\langle R_1^4 \rangle$, $\langle R_2^4 \rangle$, $\langle R_3^4 \rangle$ and $\langle (R_1^2 + R_2^2 + R_3^2)^2 \rangle$ are listed in Table 3. Using this approach it is possible to prove that the occurrence of directed motion decreases in the order NT < LAT < NCZ, only recalling that A_3 varies from 0 (circular movement) to 1 (motion along a specific direction).

Discussion

Despite the realization that DNA movement to the cell nucleus is possibly one of the most important barriers to transfection, little work has been done to characterize the mechanisms by which lipoplexes cross the dense cytoplasm to reach the nucleus. It has been suggested that the dense cytoplasmic latticework hampers free diffusion of large macromolecules, including DNA. Hence, since transfection does take place, lipoplexes must be able to cross the cytoplasm via means other than diffusion. One possibility is that lipoplexes utilize the cell's own machinery for transporting DNA through the cytoplasm: the cytoskeletal network. Understanding how lipoplexes move through the cytoplasm is imperative to understand and enhance transfection efficiencies, as well as the field of gene therapy as a whole.[37] To our knowledge, just a few studies on the role of cytoskeleton in

Table 1 MSD divisions by type according to the algorithm proposed (ESI†). D, C and B stand for directed, confined and Brownian motion, respectively

		NT	LAT	NCZ
MSD$_x$	D	41 (72%)	16 (64%)	5 (25%)
	C	2 (3.5%)	0	4 (20%)
	B	14 (24.5%)	9 (36%)	11 (55%)
MSD$_y$	D	35 (61.4%)	13 (52%)	10 (50%)
	C	1 (1.8%)	0	0
	B	21 (36.8%)	12 (48%)	10 (50%)
MSD$_z$	D	3 (5.2%)	1 (4%)	0
	C	1 (1.8%)	0	1 (5%)
	B	53 (93%)	24 (96%)	19 (95%)

Table 2 Physical parameters from unweighted fits of MSD_x, MSD_y and MSD_z. $\langle\rangle$ represents the average value. D, C and B stand for directed, confined and Brownian motion, respectively. Note that the absence of $\langle\rangle$ and the symbol * denote the presence of only one MSD curve. The symbol — denotes not detected values

			NT	LAT	NCZ
D	$\langle D_x\rangle$	$[10^{-3}\ \mu m^2\ s^{-1}]$	0.34 ± 0.27	0.77 ± 0.52	1.05 ± 0.86
	$\langle D_x\rangle$	$[10^{-3}\ \mu m^2\ s^{-1}]$	0.35 ± 0.31	0.81 ± 0.61	0.83 ± 0.71
	$\langle D_x\rangle$	$[10^{-3}\ \mu m^2\ s^{-1}]$	4.20 ± 0.31	$6.98 \pm 0.01*$	—
	$\langle v_x\rangle$	$[\mu m\ s^{-1}]$	0.032 ± 0.017	0.039 ± 0.017	0.041 ± 0.029
	$\langle v_y\rangle$	$[\mu m\ s^{-1}]$	0.035 ± 0.015	0.043 ± 0.025	0.042 ± 0.027
	$\langle v_z\rangle$	$[\mu m\ s^{-1}]$	0.092 ± 0.027	$0.091 \pm 0.004*$	—
C	$\langle D_x\rangle$	$[10^{-3}\ \mu m^2\ s^{-1}]$	1.71 ± 011	—	1.29 ± 0.53
	D_y	$[10^{-3}\ \mu m^2\ s^{-1}]$	2.73 ± 0.08	—	—
	D_z	$[10^{-3}\ \mu m^2\ s^{-1}]$	1.82 ± 0.21	—	3.54 ± 0.21
	$\langle L_x\rangle$	$[\mu m]$	0.152 ± 0.002	—	0.100 ± 0.24
	L_y	$[\mu m]$	0.140 ± 0.001	—	—
	L_z	$[\mu m]$	0.127 ± 0.002	—	0.178 ± 0.002
B	$\langle D_x\rangle$	$[10^{-3}\ \mu m^2\ s^{-1}]$	0.66 ± 0.95	1.40 ± 1.40	0.70 ± 0.42
	$\langle D_y\rangle$	$[10^{-3}\ \mu m^2\ s^{-1}]$	0.7 ± 1.0	1.09 ± 0.74	0.93 ± 0.52
	$\langle D_z\rangle$	$[10^{-3}\ \mu m^2\ s^{-1}]$	5.01 ± 5.60	10.30 ± 7.17	3.63 ± 1.69

the intracellular dynamics of lipoplexes have been reported so far.[38–40] The aim of our present work was therefore to investigate the role played by cytoskeleton in the intracellular trafficking of gene therapy non-viral vectors. As clarified above, the experimental approach we chose (*i.e.* the pharmacological disassembly of cytoskeleton structures) did not allow us to gain precise information about where in the cell tracking was accomplished. In principle, this could have some importance from a biological perspective, since different subcellular locations may give rise to distinct complex motion. However, here we specifically addressed the role of cytoskeleton in the intracellular dynamics of cationic liposome–DNA complexes, while the existence of a

relationship between lipoplex localization within specific cellular sub-regions and its dynamics will be the object of future investigations. In addition, intracellular lipoplex dynamics could be affected by the mechanism of cell entry. It has been recently clarified that macropinocytosis is the major pathway responsible for lipoplex uptake in CHO cells.[41,42] In addition, a minor pathway, probably mediated by fusion between multicomponent lipoplexes and the plasma membrane, is responsible for DNA delivery.[24] While macropinocytosis is a well-established concept, the mechanism of fusion of lipoplexes with the plasma membrane is not completely understood yet. Initially suggested as a way to deliver DNA directly into the cytoplasm, it has gradually been revised due to novel insights about the structure of lipoplexes at the nanoscale.[24,25,27–29] Synchrotron small angle X-ray scattering has unambiguously revealed that lipoplexes are often assembled in a multilamellar nanostructure made of several (from tens to a few hundreds) alternating DNA–lipid layers. The multi-lamellarity of lipoplexes has forced a reconsideration of the mechanism of fusion as somewhat different from the well-established concept of merging of a vesicle with other vesicles or a part of a cell membrane. Numerous contacts visualized by electron microscopy between lipoplexes and cellular membranes supported a concept of gradual lipoplex peeling and subsequent intracellular DNA release.[43] According to the present understanding, lipoplex fusion results in the internalization of vesicular structures with a number of lipid layers peeled off by interaction with the plasma membrane.[43] Whatever the uptake mechanism is, internalized lipoplexes are vesicles that appear as punctate structures of regular shape in a confocal image. They can be
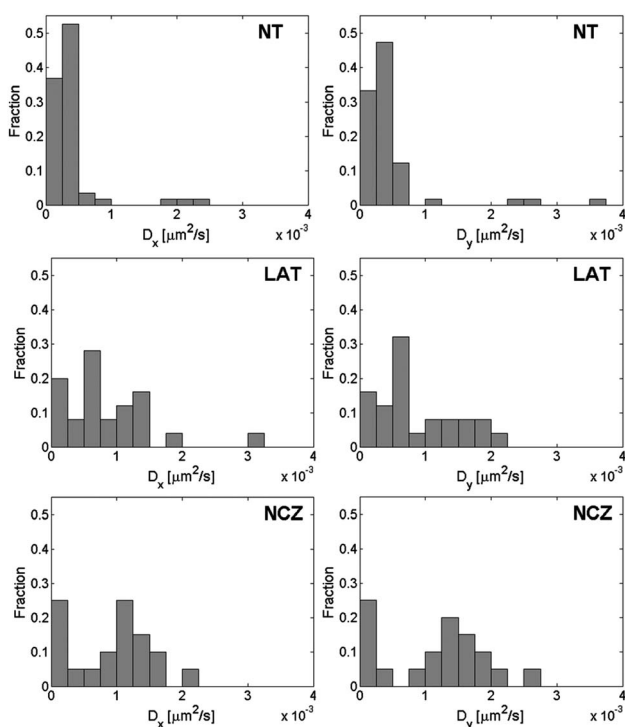
Fig. 2 Histograms of short-term diffusion coefficients $D_x(0;4)$ (left) and $D_y(0;4)$ (right) for NT, LAT and NCZ mean square displacements.

Table 3 NT, LAT and NCZ trajectories: $\langle R_1^4\rangle$, $\langle R_2^4\rangle$, $\langle R_3^4\rangle$ and $\langle(R_1^2 + R_2^2 + R_3^2)^2\rangle$ necessary to calculate A_3 (also shown)

	NT	LAT	NCZ
$\langle R_1^4\rangle$	0.000064	0.001432	0.001085
$\langle R_2^4\rangle$	0.001321	0.006731	0.004089
$\langle R_3^4\rangle$	0.160995	0.159639	0.115709
$\langle(R_1^4 + R_2^4 + R_3^4)^2\rangle$	0.186845	0.233120	0.197100
A_3	0.804	0.563	0.440

easily distinguished from diffusing halos of irregular shape due to DNA released in the cytoplasm. Since the main aim of the present work was to provide novel insights about the mechanism of lipoplex transport within CHO cells, only vesicular structures of regular shape were included in the tracking procedure. On the other hand, the traffic of material once released from the vesicular structures has not been addressed here and will be the object of future investigations. As explained in the Experimental methods section, we paid extreme attention to ensure that a lipoplex was inside the cell before tracking it.

Mean square displacement results along the optical axis seem to be less accurate than in the x and y plane, as discussed before. Thus, even if the SPT technique allowed us to follow lipoplexes in their 3D journey inside the cell, we firstly restrict our discussion to two-dimensional motions (i.e. motions in the x and y plane). In addition, in this way it is easier for us to compare our results with the ones obtained by other research groups that exclusively adopt conventional a posteriori SPT methods (mostly 2D techniques).[38–40] To address the role of actin and microtubules we first consider the occurrence of each mode of motion (Table 1). In NT cells, the percentages of each mode of motion immediately show that directed motion is the leading one.

The next step involves the comparison of cytoskeleton elements between actin filaments and microtubules. In LAT-treated and NCZ-treated cells, the percentages of directed motion prove that microtubules are the favored cytoskeleton element. In fact, even more than actin inhibition, microtubule depolymerization lowers the occurrence of directed motion (from 72% to 25% along x and from 61.4% to 50% along y) while raising in almost complementary manner the percentage of Brownian motion (from 24.5% to 55% along x and from 36.8% to 50% along y).

The presence of relatively high percentages (around 50%) of directed motion in LAT and NCZ cells might reflect the partial repolymerization of actin and microtubule networks. As stated elsewhere[39] the complete inhibition of actin polymerization lasts about 1 h while inhibition of tubulin polymerization lasts for about 2 h. To mimic transfection conditions, our SPT experiments were carried out about 4 h after inhibitor treatment, making likely the hypothesis of partial cytoskeleton repolymerization. To test this suggestion, the cytoskeleton was stained with actin-green fluorescent protein (actin-GFP) and tubulin-yellow fluorescent protein (tubulin-YFP) and its recovery was imaged as a function of time by confocal laser scanning microscopy. 4–8 hours after lipoplex administration (i.e. when SPT experiments were performed) a progressive, but never complete, reformation of cytoskeleton structures was found (representative confocal images are reported in the ESI†). Thus, it is realistic to conclude that the percentages of directed motion in LAT and NCZ cells are overestimated and actually due to lipoplexes actively transported along newly reformed cytoskeleton filaments. One may wonder why inhibitors were not added immediately before starting SPT experiments, i.e. 4 h after lipoplex administration when lipoplex internalization is assumed to be complete. In that case, the effect of inhibitors would be definitely stronger, but any effect of cytoskeleton on the lipoplex uptake would not be detectable. Thus, the experimental protocol we chose seems to be the best compromise to investigate the effect of cytoskeleton on the intracellular trafficking without

affecting the ability to examine its influence on the cellular uptake. The three dimensional asphericity A_3 supports the aforementioned conclusion of directed motion as the favored mechanism of transport. In fact, the A_3 value in NT cells moves towards unity denoting motion along a preferred direction while asphericity values in LAT and NCZ cells are ranged around the theoretical random walk value (Table 3). However, even if our results seem to be more consistent for actin filaments, it must be remembered that the theoretical random walk value is obtained in the large N limit and unfortunately we are not dealing with infinite trajectories.

A comparison with the results published in other works is mandatory. Ondrej et al.[39] demonstrated that plasmid DNA–lipid complexes bind to microtubules and show directional movement along the microtubule network, similar to viruses. So far our conclusions coincide. However, inhibiting the polymerization of microtubules, they found something different: actin filaments were found to be responsible for highly restricted diffusive motion, with corresponding slow randomly oriented movement. Sauer et al.[40] studied the dynamics of magnetic lipoplexes by conventional a posteriori SPT. Magnetic lipoplexes showed a three-phase behavior. During phase I lipoplexes were attached to the cell surface and showed slow cooperative transport behavior ruled by actin filaments. Phase II took place inside the cell and was characterized by anomalous and confined diffusion. Phase III represented active transport along microtubules inside the cell. So far our conclusions still coincide, even if we have tracked the lipoplexes while already inside the cell.

To be more quantitative it is necessary to consider our results of the unweighted fits performed according to the theoretical expressions for each mode of motion. In the following tables our derived physical parameters are given along with the results of Ondrej et al. and Sauer et al. for a better comparison. As stated above, all the resulting average parameters regarding the x and y directions lay in the same interval of values. In contrast, exclusively in the cases of directed and Brownian motion, the mean z diffusion coefficients and the mean z velocities are almost 10-fold and 3-fold higher, respectively. The Ondrej et al. tracking technique provided 3D trajectories and the results are shown considering the three dimensional diffusion coefficient and velocity, viz. $6D = 2D_x + 2D_y + 2D_z$ and $v^2 = v_x^2 + v_y^2 + v_z^2$, respectively. This leads to Table 4. In the work of Ondrej et al.[39] the confined motion is not analyzed. The comparison between the results of Ondrej et al. and our results is therefore limited to directed and Brownian motion. Even if the disruption either of actin filaments or of microtubules did not alter the complementary cytoskeletal element, the use of inhibitors made the directed motion disappear, different from our experiments. The discrepancy might be explained recalling the recovery hypothesis introduced above. In addition, when active transport occurred, the mean velocities were 10- to 100-fold smaller in the case of microtubule and actin direct transport. Ondrej et al. lastly showed how latrunculin B and nocodazole affected the Brownian motion of lipoplexes: the mean diffusion coefficient in NCZ cells remained almost equal to the one in NT cells while in LAT cells the disruption of actin filaments slowed down the diffusion. Instead, our results show that actin depolymerization speeds up the diffusion (almost without changing the mean velocity) while microtubule disruption is responsible for smaller diffusion

Table 4 Comparison of physical parameters obtained by fitting MSD curves. $\langle\rangle$ represents the average value. D and B stand for directed and Brownian motion, respectively. The symbols ×, *, † and ‡ indicate our present results, Ondrej *et al.* results,[39] Ondrej *et al.* results regarding actin filaments and Ondrej *et al.* results regarding microtubules, respectively. Distinction of motion along actin filaments or microtubules was achieved by staining the corresponding cytoskeletal element.[39] ND stands for not detected

				NT	LAT	NCZ
D	$\langle D \rangle$	$[10^{-3}\ \mu m^2\ s^{-1}]$	×	1.63 ± 0.17	2.85 ± 0.27	0.63 ± 0.37
			†	1.42 ± 0.51	ND	ND
			‡	ND	ND	ND
	$\langle v \rangle$	$[\mu m\ s^{-1}]$	×	0.104 ± 0.050	0.108 ± 0.024	0.058 ± 0.056
			†	0.005 ± 0.001	ND	ND
			‡	0.019 ± 0.001	ND	ND
B	$\langle D \rangle$	$[10^{-3}\ \mu m^2\ s^{-1}]$	×	2.12 ± 1.92	4.26 ± 2.44	1.75 ± 0.61
			*	ND	0.38 ± 0.14	1.36 ± 0.29

coefficients and velocities. In contrast to Ondrej *et al.*, it is well established that microtubule motors are responsible for the enhanced diffusion in active intracellular transport of vesicles in living fibroblasts.[44] Caspi *et al.*[44] found that microtubule depolymerization eliminates the enhanced diffusion (*i.e.* smaller diffusion coefficients), while actin depolymerization has no measurable effect. However, the intracellular cytoskeleton being a coexistence of a dilute network of microtubules with a denser F-actin network, actin depolymerization might have reduced appreciably the obstruction thus boosting the diffusion. Sauer *et al.* adopted a 2D SPT technique and the results are here presented considering the two-dimensional diffusion coefficient and velocity, *viz.* $4D = 2D_x + 2D_y$ and $v^2 = v_x^2 + v_y^2$, respectively. As done above, Table 5 is used to facilitate the comparison. The reduced accuracy in the z analysis makes it preferable to define the two-dimensional parameters considering only the x and y ones.

Furthermore, the comparison is here shown just for NT cells, completely missing the treated ones in Sauer *et al.* In the directed motion analysis, phase I and our diffusion coefficients and velocities are in good agreement. This could make us conclude the directed motion we observe derives from the actin filaments, but the lipoplexes are tracked in two different places (attached to the cell surface in Sauer *et al.* and inside the cell in our study).

Table 5 Comparison of physical parameters obtained by fitting MSD curves. $\langle\rangle$ represents the average value. D and C stand for directed and confined motion, respectively. The symbols ×, *, † and ‡ denote our present results, Sauer *et al.* results,[40] Sauer *et al.* results regarding actin filaments and Sauer *et al.* results regarding microtubules, respectively. Distinction of motion along actin filaments or microtubules was achieved by distinguishing their leading role in two different phases.[40] ND stands for not detected. $\langle L \rangle$ denotes the average between $\langle L_x \rangle$ and $\langle L_y \rangle$

				NT
D	$\langle D \rangle$	$[10^{-3}\ \mu m^2\ s^{-1}]$	×	0.35 ± 0.21
			†	0.2 ± 0.2
			‡	$10^2 \pm 10^2$
	$\langle v \rangle$	$[\mu m\ s^{-1}]$	×	0.047 ± 0.032
			†	0.015 ± 0.006
			‡	0.500 ± 0.300
C	$\langle D \rangle$	$[10^{-3}\ \mu m^2\ s^{-1}]$	×	0.98 ± 0.01
			*	ND
	$\langle L \rangle$	$[\mu m]$	×	0.0245 ± 0.0013
			*	0.1–1.3

Instead, the phase III microtubule velocity and diffusion coefficient are 10- and 1000-fold larger, respectively. Lastly, the mean size of our restricted region is 10- to 100-fold smaller. This difference might be lessened if one considers the difference between magnetic and non-magnetic (ours) lipoplex sizes (approximate diameters equal to 390 and 800 nm, respectively). In fact, in both experimental methods it is the 'center of mass' and not the whole particle to be tracked leading to an actual size of the restricted region that is approximately the sum of the measured size and the radius of the tracked particle.

Furthermore, it is accepted that the major part of active transport takes place on associating with endosomes. One possible conclusion that can be reached is that the speed of microtubule-dependent transport may be slowed down by loading highly dense nanocarriers. Thus, it is obvious to conclude that carrier loading causes a slowing of endosome trafficking. According to the literature, an alternative explanation is that the speed of intracellular lipoplex transport varies depending on the cellular uptake mechanism. It has recently been shown that cholesterol-dependent macropinocytosis is the major pathway responsible for cellular uptake of lipoplexes.[41] Therefore, the slow transport rate may reflect the trafficking of macropinocytosis. To confirm such a suggestion, further experiments are needed.

Experimental methods

Cationic liposome preparation

The cationic lipids 1,2-dioleoyl-3-trimethylammonium-propane (DOTAP) and 3β-[*N*-(*N'*,*N'*-dimethylaminoethane)-carbamoyl]-cholesterol (DC-Chol) and the zwitterionic helper lipids dioleoylphosphocholine (DOPC) and dioleoylphosphatidylethanolamine (DOPE) were purchased from Avanti Polar Lipids (Alabaster, AL) and used without further purification. DOTAP–DOPC and DC-Chol–DOPE CLs were prepared according to the following protocol. In brief, binary mixtures, at molar fractions of neutral lipid in the bilayer ϕ = neutral/cationic (mol/mol) = 0.5, were dissolved in chloroform, and the solvent was evaporated under vacuum for at least 24 h. The obtained lipid films were hydrated with the appropriate amount of Nanopure water to achieve a concentration of ~1 mg ml^{-1}. The obtained dispersions were sonicated to clarity to obtain unilamellar CLs.

Lipoplex preparation

To form MC lipoplexes (DOTAP–DOPC–DC-Chol–DOPE/pDNA) for administration to CHO-K1 cells, 100 µl of PBS were added to a dispersion containing 5 µl of DOTAP–DOPC and 5 µl of DC-Chol–DOPE CLs. The same amount of buffer was added to 1 µl of plasmid DNA (pDNA). These solutions were equilibrated for a few minutes. Then, the pDNA solution was poured into the liposome dispersion and after 20 minutes the complexes were ready to use. Fluorescein-labeled plasmids DNA (2.7 kbp, double stranded, circular plasmid), supplied at 0.5 µg µl^{-1} in a 10 mM Tris–HCl and 1 mM EDTA buffer (pH 7.5), was purchased from Mirus Bio (Madison, WI).

Cell culture and cell transfection

Chinese hamster ovary (CHO) cells are a cell line derived from the ovary of the Chinese hamster. CHO-K1 cells, derived from the original cell lines, contain a slightly lower amount of DNA. They were cultured in Dulbecco's modified Eagle's medium (DMEM) (Invitrogen, Carlsbad, CA) supplemented with 1% penicillin–streptomycin (Invitrogen, Carlsbad, CA) and 10% fetal bovine serum (FBS) (Invitrogen, Carlsbad, CA) at 37 °C in a 5% CO_2 atmosphere, splitting the cells every 2–4 days to maintain monolayer coverage. On the day of transfection, the medium containing serum (DMEM plus FBS) was removed from the well plates that were washed three times with ∼2 ml of PBS before adding MC lipoplexes and DMEM, for a total volume of about 2 ml. After administration, the cells were incubated for 4 hours to allow complete internalization of the lipoplexes. To eliminate non-internalized and freely diffusing lipoplexes, the medium was then replaced with a medium containing 200 µl of DiIC18(3) (Invitrogen, Carlsbad, CA), a lipophilic membrane stain that helped the localization of a single lipoplex inside the cell during the tracking routine (*i.e.* to ensure that the lipoplex was inside the plasma membrane, a 2D frame was scanned before each tracking cycle). After only 15 minutes, the medium was at last replaced with the measurement medium, DMEM depleted of red phenol. When cells were treated with latrunculin B and nocodazole, both purchased from Sigma-Aldrich (St Louis, MO), the procedure was slightly different. Before lipoplex administration, cells were first incubated for not more than 15 minutes with a 20 µM latrunculin B or nocodazole medium and then washed three times with ∼2 ml of PBS. Concentrations and incubation times were chosen according to the literature.[15,30] To investigate the cytoskeleton recovery after inhibitor treatments, actin filaments and microtubules were fluorescently labeled. Thus, CHO cells were transfected with actin-GFP or tubulin-YFP (Clontech, Palo Alto, CA, USA), using Lipofectamine 2000 (Invitrogen, Carlsbad, CA, USA).

Microscopy experiments

Two-photon microscopy experiments were carried out using a Zeiss Axiovert 135 TV microscope. The excitation source was a mode-locked Ti:sapphire laser (Mai Tai HP with integrated Millennia, Spectra-Physics, Santa Clara, CA) tuned at 790 nm. Detailed experimental conditions can be found elsewhere.[20–23] The experiments were controlled by custom-made data acquisition software (SimFCS, Laboratory for Fluorescence Dynamics,

Irvine, CA). This software, which also contains some of the tools used for trajectory analysis, can be downloaded from the Laboratory for Fluorescence Dynamics website (www.lfd.uci.edu). In addition, a custom-made Matlab (The MathWorks, Natick, MA) program was used for the data analysis.

Tracking procedure

The theory of three-dimensional single particle tracking is fully described elsewhere.[31–33] During each cycle of tracking, the excitation beam traces a given number of circular orbits surrounding the particle of interest and the fluorescence intensity is integrated at different points along the orbit. The determination of the particle position is done on the fly by analyzing the fast Fourier transform of the intensity of the signal.[31] Before the next cycle of tracking, the center of scanning is moved to the position determined for the particle in the previous cycle.

Analysis of single-particle trajectories

Mean square displacement (MSD) and gyration tensor (T) have been calculated directly from the trajectory coordinates. From the experimental time sequence [$x_n = x(n\delta t)$, $y_n = y(n\delta t)$, $z_n = z(n\delta t)$, $n = 0, 1, 2,...N$] with δt being the data acquisition time interval, the one-dimensional mean square displacements (MSD_x, MSD_y, MSD_z) have been calculated averaging over all pairs (of points that are $n\delta t$ time steps apart) [eqn (1)–(3)].

$$MSD_x(n\delta t) = \frac{1}{N-n+1}\sum_{i=0}^{N-n}(x_{i+n}-x_i)^2 \qquad (1)$$

$$MSD_y(n\delta t) = \frac{1}{N-n+1}\sum_{i=0}^{N-n}(y_{i+n}-y_i)^2 \qquad (2)$$

$$MSD_z(n\delta t) = \frac{1}{N-n+1}\sum_{i=0}^{N-n}(z_{i+n}-z_i)^2 \qquad (3)$$

where N is the total number of trajectory points and $n\delta t$ is the time lag τ.

The calculated MSDs could be fitted using theoretical expressions for each mode of motion that might characterize the lipoplex intracellular trafficking. Eqn (4)–(6) represent the theoretical one-dimensional mean square displacements when the lipoplex undergoes Brownian diffusion, confined diffusion and directed diffusion, respectively.

$$MSD_\alpha(\tau) = 2D_\alpha\tau \qquad (4)$$

$$MSD_\alpha(\tau) = 2D_\alpha\tau + v_\alpha^2\tau^2 \qquad (5)$$

$$MSD_\alpha(\tau) \approx \frac{L_\alpha^2}{6}\left\{1 - \frac{96}{\pi^4}\exp\left[-\frac{\pi^2 D_\alpha}{L_\alpha^2}\tau\right]\right\} \qquad (6)$$

where $\alpha = x$, y, z and D_α, L_α and v_α are the one-dimensional diffusion coefficient, the size of the restricted region and the velocity, respectively. Because diffusion is a stochastic process, even with infinitely precise measurements of positions the calculated mean square displacement (MSD), and the diffusion coefficient and drift rate derived therefrom, will have

theoretically expected statistical variances. Therefore, an estimate of statistical accuracy has been essential for our analysis. In the case of Brownian diffusion, for instance, a good estimate for the relative error in D_α was obtained by Qian *et al.*[34] and it is $\sim[2m/3(N-m)]^{1/2}$ (where m is the maximum lag time that is considered). From this it easily follows that fitting the experimental MSD using eqn (4) is not accurate at all. It is then necessary to set a proper maximum time lag in order to limit the uncertainty. Taking into account the wide range of trajectory lengths, we decided to set $m = 49$ that yields a relative error less than 27%. After that and prior to performing the fitting, a simple division by type (Brownian motion, confined motion and directed motion) can be easily achieved. The procedure we used is explained in the ESI†. Another trajectory analysis involves the calculation of the gyration tensor, T. Given the principal radii of gyration (*i.e.* the eigenvalues of T), Rudnick and Gaspari[35] defined a parameter A_3 which measures the asphericity of a trajectory and thereby provides a useful description of deviations from spherical symmetry (ESI†).

Conclusions

In summary our 3D SPT results have clarified that, even though both types of cytoskeleton structure could play a role in gene delivery, microtubules are the preferential network for the active transportation of cationic liposome–DNA complexes. The physical and time trajectories of single genetic particles, the direct visualization of interactions between these particles and cellular machinery, and the transient dynamic information revealed by the time trajectories can provide critical insights, complementary to ensemble measurement results, into the molecular mechanisms underlying the trafficking of genetic materials in cells. Future experiments will attempt to provide a better knowledge of the lipoplex intracellular trafficking within specific subcellular regions, assessing the effects of other relevant physico-chemical parameters such as lipoplex phase[16,45] and size,[15,46] membrane charge density,[47–50] lipid composition[51] and hydration.[52]

Acknowledgements

Notes and references

1 T. Friedmann and R. Roblin, *Science*, 1972, **175**, 949–955.
2 M. Cavazzana-Calvo, S. Hacein-Bey, G. S. Basile, F. Gross, E. Yvon, P. Nusbaum, F. Selz, C. Hue, S. Certain, J. L. Casanova, P. Bousso, F. Le Deist and A. Fischer, *Science*, 2000, **288**, 669–672.
3 A. C. Boyda, *Cystic Fibrosis in the 21st Century*, 2006, vol. 34, pp. 221–229.
4 M. G. Kaplitt, A. Feigin, C. Tang, H. L. Fitzsimons, P. Mattis, P. A. Lawlor, R. J. Bland, D. Young, K. Strybing, D. Eidelberg and M. J. During, *Lancet*, 2007, **369**, 2097–2105.
5 Z. Z. Yang, H. F. Wang, J. Zhao, Y. Y. Peng, J. Wang, B. A. Guinn and L. Q. Huang, *Cancer Gene Ther.*, 2007, **14**, 599–615.
6 F. Liu and L. Huang, *J. Controlled Release*, 2002, **78**, 259–266.
7 P. L. Felgner, T. R. Gadek, M. Holm, R. Roman, H. W. Chan, M. Wenz, J. P. Northrop, G. M. Ringold and M. Danielsen, *Proc. Natl. Acad. Sci. U. S. A.*, 1987, **84**, 7413–7417.
8 D. Ferber, *Science*, 2001, **294**, 1638–1642.
9 S. Hacein-Bey-Abina, C. von Kalle, M. Schmidt, F. Le Deist, N. Wulffraat, E. McIntyre, I. Radford, J. L. Villeval, C. C. Fraser, M. Cavazzana-Calvo and A. Fischer, *N. Engl. J. Med.*, 2003, **348**, 255–256.
10 N. B. Woods, V. Bottero, M. Schmidt, C. Von Kalle and I. M. Verma, *Nature*, 2006, **440**, 1123.
11 A. R. Thierry, S. Abes, S. Resina, A. Travo, J. P. Richard, P. Prevot and B. Lebleu, *Biochim. Biophys. Acta, Biomembr.*, 2006, **1758**, 364–374.
12 P. Midoux, C. Pichon, J. J. Yaouanc and P. A. Jaffrès, *Br. J. Pharmacol.*, 2009, **157**, 166–178.
13 I. A. Khalil, K. Kogure, H. Akita and H. Harashima, *Pharmacol. Rev.*, 2006, **58**, 32–45.
14 R. Koynova and R. C. MacDonald, *Biochim. Biophys. Acta, Biomembr.*, 2005, **1714**, 63–70.
15 I. S. Zuhorn, R. Kalicharan and D. Hoekstra, *J. Biol. Chem.*, 2002, **277**, 18021–18028.
16 I. S. Zuhorn, U. Bakowsky, E. Polushkin, W. H. Visser, M. C. A. Stuart, J. B. F. N. Engberts and D. Hoekstra, *Mol. Ther.*, 2005, **11**, 801–810.
17 G. L. Lukacs, P. Haggie, O. Seksek, D. Lechardeur, N. Freedman and A. S. Verkman, *J. Biol. Chem.*, 2000, **275**, 1625–1629.
18 N. D. Van Loo, E. Fortunati, E. Ehlert, M. Rabelink, F. Grosveld and B. J. Scholte, *J. Virol.*, 2001, **75**, 961–970.
19 G. E. Lee, J. W. Murray, A. W. Wolkoff and D. W. Wilson, *J. Virol.*, 2006, **80**, 4264–4275.
20 V. Levi, A. S. Serpinskaya, E. Gratton and V. Gelfand, *Biophys. J.*, 2006, **90**, 318–327.
21 V. Levi, V. I. Gelfand, A. S. Serpinskaya and E. Gratton, *Biophys. J.*, 2006, **90**, L07–L09.
22 V. Levi and E. Gratton, *Cell Biochem. Biophys.*, 2007, **48**, 1–15.
23 V. Levi and E. Gratton, *Chromosome Res.*, 2008, **16**, 439–449.
24 C. Marchini, D. Pozzi, M. Montani, C. Alfonsi, A. Amici, S. Candeloro De Sanctis, M. A. Digman, S. Sanchez, E. Gratton, H. Amenitsch, A. Fabbretti, C. O. Gualerzi and G. Caracciolo, *Cancer Gene Ther.*, 2011, **18**, 543–552.
25 C. Marchini, D. Pozzi, C. Alfonsi, M. Montani, A. Amici, H. Amenitsch and G. Caracciolo, *Langmuir*, 2010, **26**, 13867–13873.
26 G. Caracciolo, R. Caminiti, M. A. Digman, E. Gratton and S. Sanchez, *J. Phys. Chem. B*, 2009, **113**, 4995–4997.
27 G. Caracciolo, D. Pozzi, R. Caminiti, C. Marchini, M. Montani, A. Amici and H. Amenitsch, *J. Phys. Chem. B*, 2008, **112**, 11298–11304.
28 G. Caracciolo, D. Pozzi, R. Caminiti, C. Marchini, M. Montani, A. Amici and H. Amenitsch, *Biochim. Biophys. Acta, Biomembr.*, 2007, **1768**, 2280–2292.
29 G. Caracciolo, D. Pozzi, R. Caminiti and H. Amenitsch, *Appl. Phys. Lett.*, 2005, **87**, 133901.
30 J. Rejman, A. Bragonzi and M. Conese, *Mol. Ther.*, 2005, **12**, 468–474.
31 K. Kis-Petikova and E. Gratton, *Microsc. Res. Tech.*, 2004, **63**, 34–49.
32 V. Levi, Q. Q. Ruan and E. Gratton, *Biophys. J.*, 2005, **88**, 2919–2928.
33 V. Levi, Q. Q. Ruan, M. Plutz, A. S. Belmont and E. Gratton, *Biophys. J.*, 2005, **89**, 4275–4285.
34 H. Qian, M. P. Sheetz and E. L. Elson, *Biophys. J.*, 1991, **60**, 910–921.
35 J. Rudnick and G. Gaspari, *J. Phys. A: Math. Gen.*, 1986, **19**, L191–L193.
36 C. Hellriegel and E. Gratton, *J. R. Soc. Interface*, 2009, **6**, S3–S14.
37 E. E. Vaughan and D. A. Dean, *Mol. Ther.*, 2006, **13**, 422–428.
38 N. Ruthardt, D. C. Lamb and C. Bräuchle, *Mol. Ther.*, 2011, **19**, 1199–1211.
39 V. Ondrej, E. Lukasova, M. Falk and S. Kozubek, *Acta Biochim. Pol.*, 2007, **54**, 657–663.
40 A. M. Sauer, K. G. de Bruin, N. Ruthardt, O. Mykhaylyk, C. Plank and C. Bräuchle, *J. Controlled Release*, 2009, **137**, 136–145.
41 F. Cardarelli, D. Pozzi, C. Marchini, A. Bifone and G. Caracciolo, *Mol. Pharmaceutics*, 2012, **9**, 334–340.
42 X. Zhang, P. G. Allen and M. Grinstaf, *Mol. Pharmaceutics*, 2012, **8**, 758–766.
43 R. Koynova, Y. Tarahovsky, L. Wang and R. C. MacDonald, *Biochim. Biophys. Acta*, 2007, **1768**, 375–386.

44 A. Caspi, R. Granek and M. Elbaum, *Phys. Rev. Lett.*, 2000, **85**, 5655–5658.

45 G. Caracciolo and R. Caminiti, *Chem. Phys. Lett.*, 2005, **411**, 327–332.

46 G. Caracciolo, L. Callipo, S. Candeloro De Sanctis, C. Cavaliere, D. Pozzi and A. Laganà, *Biochim. Biophys. Acta*, 2010, **1798**, 536–543.

47 G. Caracciolo, D. Pozzi, A. L. Capriotti, C. Cavaliere, P. Foglia, H. Amenitsch and A. Laganà, *Langmuir*, 2011, **27**, 15048–15053.

48 G. Caracciolo, D. Pozzi, S. Candeloro De Sanctis, A. L. Capriotti, G. Caruso, R. Samperi and A. Laganà, *Appl. Phys. Lett.*, 2011, **99**, 033702.

49 G. Caracciolo, D. Pozzi, H. Amenitsch and R. Caminiti, *Langmuir*, 2007, **23**, 8713–8717.

50 M. Muñoz-Úbeda, S. K. Misra, A. L. Barrán-Berdón, C. Aicart-Ramos, M. B. Sierra, J. Biswas, P. Kondaiah, E. Junquera, S. Bhattacharya and E. Aicart, *J. Am. Chem. Soc.*, 2011, **133**, 18014–18017.

51 M. Ramezani, M. Khoshhamdam, A. Dehshahri and B. Malaekeh-Nikouei, *Colloids Surf., B*, 2009, **72**, 1–5.

52 D. Pozzi, H. Amenitsch, R. Caminiti and G. Caracciolo, *Chem. Phys. Lett.*, 2005, **422**, 439–445.

Addition and correction

Note from RSC Publishing

This article was originally published with incorrect page numbers. This is the corrected, final version.

The Royal Society of Chemistry apologises for these errors and any consequent inconvenience to authors and readers.